

THERMAL BEHAVIOR OF TISSUES HAVING DIFFERENT POROSITIES DURING CONTINUOUS CO₂ LASER IRRADIATION

by

Khaled S. SHIBIB** and *Mohammed A. MUNSHID

Department of Laser and Optoelectronics, University of Technology,
Baghdad, Iraq

Original scientific paper
UDC: 617-7:544.032.65:517.96
DOI: 10.2298/TSCI1001049S

The using of CO₂ laser in operation room has been intensified in last few decades, requiring deep insight into the thermal behavior of tissue subjected to laser beam. Using CO₂ laser as a scalpel is studied here, with temperature distribution, char depth and velocity of ablation obtained numerically for different porosities. A moving finite element mesh has been used with an iterative solution procedure based on a band matrix solver. The effect of porosity for different type of tissues is studied for lasers with different power intensities. Some conclusions have been reached; a reduction in char layer depth can be obtained as power intensity increase; also for the same laser power as porosity increases the char depth may decrease. A good agreement of the results with typical experimental data is obtained which verifies the proposed method of solution.

Key words: *finite element method, laser tissue ablation, chars depth, porosity, tissue thermal behavior*

Introduction

Recently lasers have become powerful and indispensable tools, used in almost every aspect of technology. In particular, the application of laser in medicine has increased due to the development of new laser treatment technique, especially the development of a fiber that can transmit the high power laser such as CO₂ laser. A fiber made of polycrystalline silver halides of a diameter of 900 μm with 6 m in length, which is highly transparent in infrared region (3-30 μm), has been recently used to enable CO₂ laser power of up to 50 W, which can be used clinically and open a wide gate to use this type of laser in operation room [1]. In addition to this, the CO₂ laser is known to be one of the most suitable types of laser that can be used in medicine because it absorbs very superficially in tissues, and high power can be achieved, enabling its application as a scalpel in tissue cutting. The advantages beyond these are that the cutting is clean, precise, having minimum thermal damage and fast sealing of a blood vessel [2].

A deep insight into the process of laser tissue interaction is that as photons hit the tissue some will be reflected, some will enter the surface which will either absorbed, scattered or trans-

* Corresponding author; e-mail: assprofkh@coolgoose.com

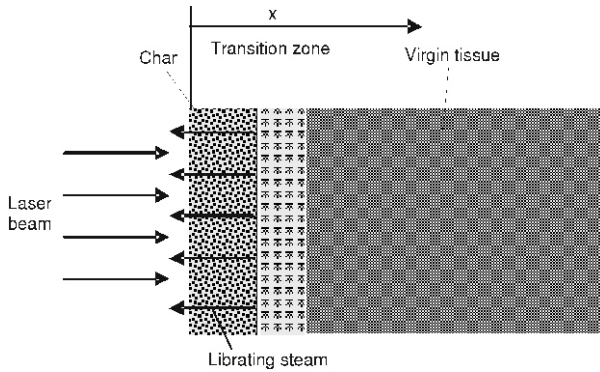


Figure 1. Schematic diagram of laser tissue interaction

layer of steam will start to move inside the tissue as heating is continued, leaving a char layer. Figure 1 shows different layers in tissue subjected to CO₂ laser. Char ablation phenomena will be established after the char had absorbed the heat of ablation causing its surface to move in depth. Voids inside char layer will be filled by the liberating steam before the steam leaves the char surface.

Theory

Partial differential equation and boundary conditions

The partial differential equation that covers this case can be used as that of composite material where two regions can be observed, the virgin and char layer, also keeping in mind the transition layer [3]:

$$k_k \frac{\partial^2 T}{\partial x^2} = \dot{m}_{wv} c_{wv} \frac{\partial T}{\partial x} + \rho_k c_k \frac{\partial T}{\partial x} \quad (1)$$

where $k = 1, n$ (n is number of regions). This equation represent a good approximation for the composite material having a dense pore spacing and small pore diameter, which is the case here.

One-dimensional field can be assumed as long as the diameter of the laser that hit the surface is significantly greater than the affected zone; which is the case here (the beam diameter is 400 μm while the affected zone is less than 100 μm). The thermal properties of two zones are, [4]:

$$k_1 = k_c \frac{1-p}{2} + k_v \frac{(1-p)^2}{2} \quad (2)$$

$$k_2 = k_v \quad (3)$$

$$\rho_1 c_1 = \rho_c c_c (1-p) + \rho_{wv} c_{wv} p \quad (4)$$

$$\rho_2 c_2 = \rho_v c_v \quad (5)$$

For the transition element the contribution of each region in the element has been taken into account as long as the front position of water evaporation is known. Also since the pore di-

mitted. This process depend mainly on laser parameters and type of tissue. The deposition of heat in tissue is due only to light (photons) that is absorbed in the tissue. For CW CO₂ laser, the absorb photons are the main part of induced laser photons which will cause a rapid increase in tissue temperature where many event may occur such as hyperthermia, denaturation of proteins, collagen which leads to coagulation of tissue, and necrosis of cells until water evaporation limit is reached. Thus, the water in tissue will evaporate and a

ameter ($6\ \mu\text{m}$) is less than the wave length of laser ($10.6\ \mu\text{m}$), the heat generation can be approximated as heat addition at the wall [4], simplifying the solution and the heat can be assumed as heat adding to the surface, so the boundary condition at air carbon interface is [4]:

$$q_s = k \left. \frac{\partial T}{\partial x} \right|_{x=0} = q = \dot{m}_c H_c = (h_{co} + h_r)(T_s - T_\infty) \quad (6)$$

where

$$\dot{m}_c = (1 - p)\rho_c V_c \quad (6a)$$

$$V_c = a_c \exp \left(-\frac{H_c M_c}{RT_c} \right) \quad (6b)$$

$$h_{co} = 25 \frac{w}{\text{m}^2\text{K}}, \text{ [5], while } h_r = 4\sigma\varepsilon \frac{T_s + T_\infty}{2} \quad (6c)$$

$$h = h_{co} + h_r \quad (6d)$$

The velocity of evaporation interface can be obtained from [4]:

$$V_w = a_w \exp \left(-\frac{H_w M_w}{RT_w} \right) \quad (7)$$

where the molecular flow concept is applicable. The internal boundary condition of water evaporation can be incorporate into the solution domain by knowing where its front is. This can be determined by knowing the velocity of evaporation from eq. (7) from which the location and element involved can be estimated. Once the element involved is determined, at the evaporation interface one can write [3]:

$$k \left. \frac{\partial T}{\partial x_x} \right|_{x_x} = k \left. \frac{\partial T}{\partial x_x} \right|_{x_x} + \dot{m}_w H_w \quad (8)$$

where

$$\dot{m}_w = w\rho_w V_w \quad (8a)$$

and

$$\dot{m}_{wv} = \dot{m}_w \quad (8b)$$

The solution can be carried out with firstly assumed former temperature distribution, incorporating the predetermined velocities into the solution, so that new temperature distribution can be predicated and a repeated step will carried out at the average temperatures till a tolerance is achieved.

Finite element formulation and method of solution

The space-wise discretization of the heat equation, subjected to the above boundary conditions can be accomplished using Galerkin method. The volume of interest Ω is divided

into a number of elements, Ω^e , with usual shape function N_i associated with each node, resulting in a system of ordinary differential equations of the form [7]:

$$[C]\dot{\bar{T}} + [K]\bar{T} = [\bar{F}] \quad (9)$$

where

$$\dot{\bar{T}} = \begin{bmatrix} \frac{\partial T_1}{\partial t} \\ \frac{\partial T_2}{\partial t} \\ \dots \\ \frac{\partial T_{NN}}{\partial t} \end{bmatrix}, \quad \bar{T} = \begin{bmatrix} T_1 \\ T_2 \\ \dots \\ T_{NN} \end{bmatrix}, \quad [\bar{F}] = \begin{bmatrix} F_1 \\ F_2 \\ \dots \\ F_{NN} \end{bmatrix}$$

The typical matrix elements are:

$$K_{ij} = \int_{\Omega^e} k_k \frac{\partial N_i}{\partial x} \frac{\partial N_j}{\partial x} d\Omega + \int_{\Omega^e} \dot{m}_{wv} C_{wv} N_i \frac{\partial N_j}{\partial x} d\Omega + \int_{\Gamma^e} N_i N_j h d\Gamma \quad (10)$$

$$C_{ij} = \int_{\Omega^e} \rho_k C_k N_i N_j d\Omega \quad (11)$$

$$F_i = \int_{\Gamma^e} N_i (q_s - hT_4) d\Gamma \quad (12)$$

in the above, the summation are taken over the contribution of each element, Ω^e , in the element volume and Γ^e refers only to the element with interface boundary on which surface condition is applied. The application of weighted residual theory to eq. (9) results in the following matrix form of:

$$\frac{[C]}{\Delta t} \Theta [K] \bar{T}_{n+1} - \frac{[C]}{\Delta t} (1 - \Theta) [K] \bar{T}_n = \bar{F} \quad (13)$$

where

$$\bar{F} = \bar{F}_{n+1} \Theta + \bar{F}_n (1 - \Theta) \quad (13a)$$

with coefficient Θ having different values, defining forward or backward solution procedure. In this solution a forward difference is carried out in an iterative pattern.

A special attention has to be paid to the location of absorption of the latent heat of water evaporation. When using the finite element equations, the effect of absorbing latent heat can be applied at the involved element nodes even it may be not applied at the surface is follows:

$$\int_{\Gamma} N^T w \rho_w H_w V_w d\Gamma = \frac{N_i}{N_j} w \rho_w H_w V_w \quad (14)$$

where unit surface area is assumed, and the integration is carried out with the shape functions out of surface of integration. Once the location is found from the pre-determined velocity, the values of shape function can be found at each time step and the eq. (14) is used to carry out the effect of latent water heat at moving positions.

Out of many possibilities to solve the Stefan problem, a reducing mesh procedure is used in this work, where the mesh is reduced by an element when the char surface ablated depth is exceeding half length of the first element where an interpolation for new mesh location and temperature can be determined simply. All these steps are carried out while the surface temperature remains the same from the previous mesh.

The region studied is divided to 499 elements and 500 nodes, with high concentration of nodes near the surface due to localized high power intensity there. A quit simple mathematical equation can represent the nodes coordinate to achieve nodes concentration near the surface which can be written as:

$$X_J = \frac{(J-1)L}{NE} \exp\left(-\frac{(NN-J)}{NE}\right) \quad (15)$$

The solution is carried out with small time step (10 μs) with a band solver technique. A result has been tested for different types of tissue which usually have a porosity between 0.7 to 0.9, and the thermal properties is taken from [8], depending on water content.

Results and discussion

As mentioned, the tissue porosity can have different values, typically between 0.7 and 0.9, being used here to test their response to laser radiation. The temperature distribution has been obtained numerically where the task is to reach the quasi-steady-state which seems to be reduced as power increases. Figure 2 indicates surface and evaporation temperature vs. power intensity at various porosities; it is obvious that as power intensity increases surface and evaporation temperature increase as well. The extent of ablation temperature increase is much greater than that of the evaporation temperature. Assuming the dissipation of heat is being limited mainly by the thermal properties of the virgin tissue, where convection and radiation loss is small comparing with other parameters, the char temperature will increase as power intensity increases, which can be seen by observing char surface temperature in fig. 2. The influence of increasing porosity is also shown in

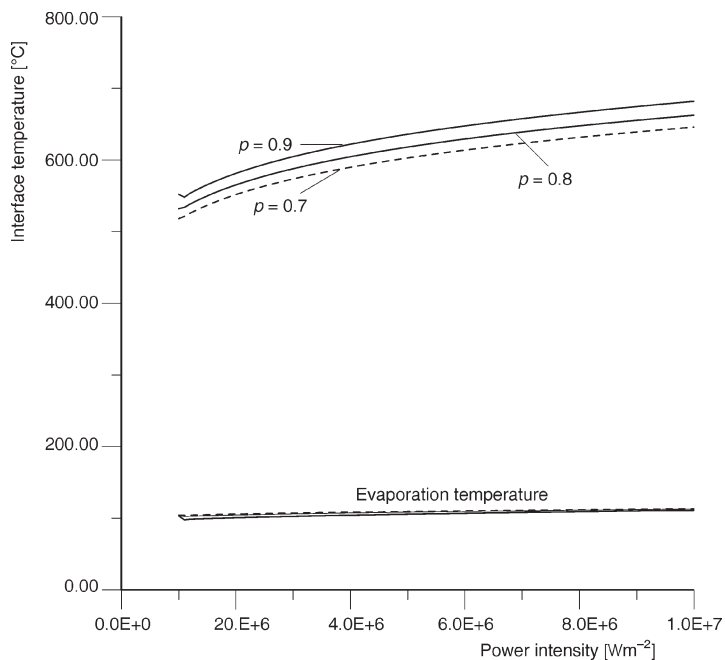


Figure 2. Surface and evaporation temperature variation with power intensity and porosity

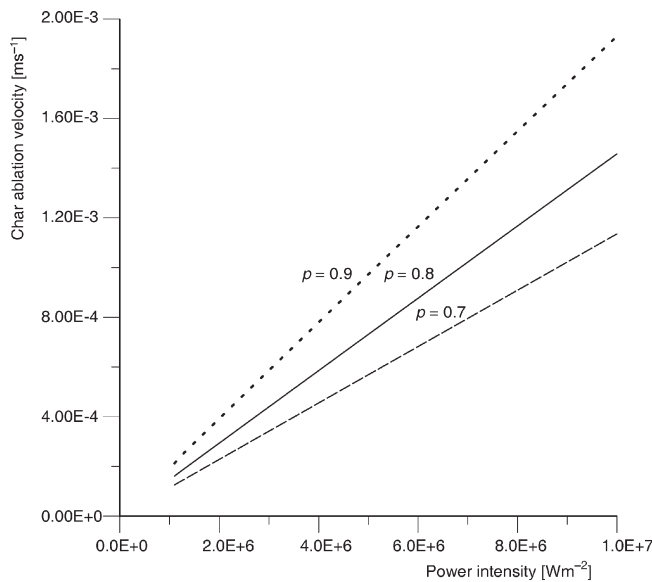


Figure 3. Ablation velocity variation with power intensity and porosity

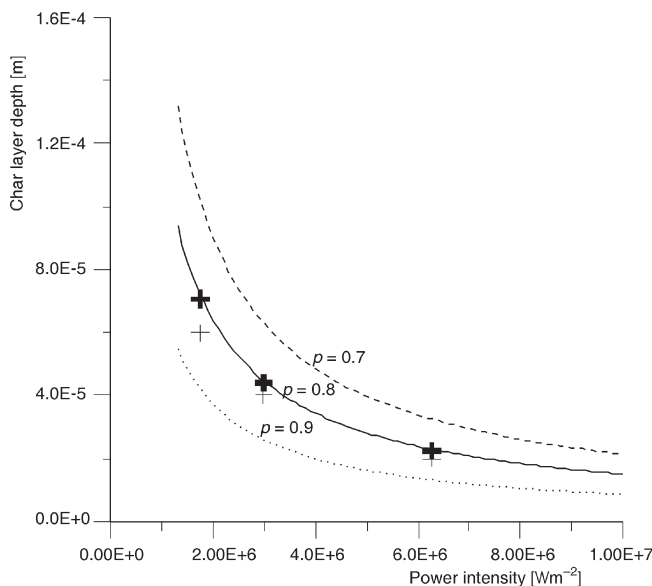


Figure 4. Char layer depth variation with power intensity and porosity, the bold plus is referred to numerical method suggested by [9]. The thin plus referred to experimental data given by [9]

fig. 2 indicating that as porosity increases for a certain power intensity the surface temperature increases as well; this is due to decrease in the effective thermal conductivity of the char layer which is composed of carbon and steam.

An increase in surface temperature will dramatically increase the velocity of ablation, fig. 3, having in mind that the increase in porosity means higher void content in char layer, reducing the effective thermal conductivity, which results in high surface temperature with high ablation rate of char layer, as shown in fig. 3. It is to be noted that at the quasi-steady-state, the ablation velocity is equal to evaporation velocity; this condition being necessary to achieve quasi-steady-state.

Figure 4 represents char depth layer vs. power intensity, assuming a good contact is maintained between char layer and virgin material. One can see that as power increases, the char layer reduces. Explanation of this phenomenon is that for low power intensity the front position of evaporation will progress inside the tissue where the rate of char ablation is slow (this is due to low rate of char surface temperature increase assuming that heat of carbon ablation is approximately four times larger than that of water evaporation), so that larger distance can be reached between the two fronts positions before quasi-steady-state is established. Vice-versa, for the high power intensity where this distance is reduced due to high ablation rate of char with a shorter dis-

tance established before a quasi-steady-state can be reached. The influence of increasing porosity seems to reduce the char layer depth. Increasing in water vapor mass flow rate means carrying more heat out of the char layer as they escape from the surface; this effect is working as a heat barrier and may decrease the temperature distribution including surface temperature, but the decrease in effective thermal conductivity seems to be more dominate than that of escaping water vapor mass flow rate, so the depth of char layer will be reduced as porosity increases. These facts are verified in figs. 2-4.

Conclusions

The solution using finite element method with reducing mesh is proved to provide a good agreement of results comparing with numerical and experimental results obtained by Zho *et al.* [9] for the tissue with same thermal properties and porosity of 0.8. This may give confidence to the results of this work where different porosities are assumed. The discrepancy between theoretical result and experimental data are due to:

- the scarce data for thermal properties of tissue and char and their variations with temperature,
- the limitation of one-dimensional model, and
- the model used to describe the heat adding at the surface.

A significant phenomenon shown in this paper is that as power intensity increase, the depth of char layer is reduced. This may provide important information to a surgeon when the char layer thickness is a disadvantage, a tissue with high porosity will have a thinner char layer than a tissue with less porosity for the same power intensity. This may be an indication to surgeons who dealing with such type of tissues on how and in what power one can deal with different type of tissues.

Nomenclature

| | |
|-----------|--|
| a | – sound velocity [ms^{-1}] |
| c | – specific heat [$\text{Jkg}^{-1}\text{K}^{-1}$] |
| d | – pore diameter [m] |
| H | – enthalpy of evaporation for water and sublimation for char [Jkg^{-1}] |
| h | – convection heat transfer coefficient [$\text{Wm}^{-2}\text{K}^{-1}$] |
| J | – integer represented current node number |
| k | – thermal conductivity [$\text{Wm}^{-1}\text{K}^{-1}$] |
| L | – original depth [m] |
| M | – molecular weight [kg kgmol^{-1}] |
| \dot{m} | – mass flow rate [$\text{kgs}^{-1}\text{m}^{-2}$] |
| N | – shape function |
| NE | – total number of element |
| NN | – total number of node |
| N^T | – column matrix for shape function |
| p | – porosity |
| q | – heat flux [Wm^{-2}] |
| R | – universal gas constant [$\text{Jkgmole}^{-1}\text{K}^{-1}$] |
| T | – temperature [$^{\circ}\text{C}$] |
| V | – velocity [ms^{-1}] |
| w | – water content |
| x | – dimension variable [m] |

Greek letters

| | |
|---------------|---------------------------------|
| δ | – char layer depth [m] |
| ε | – emissivity |
| ρ | – density [kgm^{-3}] |
| σ | – Stefan-Boltzmann constant |

Subscripts

| | |
|----------|-------------------|
| c | – carbon |
| co | – convection |
| k | – number of layer |
| r | – radiation |
| s | – char surface |
| v | – virgin |
| w | – water |
| wv | – water vapor |
| ∞ | – environmental |
| 1 | – char layer |
| 2 | – virgin layer |

References

- [1] Hamed, M., Nadeau, V., Dickinson, M. R., A Novel Modeling and Experimental Technique to Predict and Measure Tissue Temperature During CO₂ Laser Stimuli for Human Pain Studies, *J. Lasers Med. Sci.*, 21 (2006), 2, pp. 95-100
- [2] Sobol, E. N., Makropoulou, M., Serafetinides, A. A., Theoretical Model of CO₂ Laser Ablation of Soft-Tissue Phantoms, *Il Nuovo Cimento D*, 18 (1996), 4, pp. 483-490
- [3] Kanevce, Lj. P., Kanevce, G., H., Angelevski, Z. Z., Comparison of Two Kinds of Experiments for Estimation of Thermal Properties of Ablative Composite, *Proceedings*, 3rd International Conference on Inverse Problems in Engineering, ASME, Washington, USA, 1999, pp. 13-18
- [4] Vasiliev, V. N., Serkov, S. K., Biological Tissue Destruction under Laser Irradiation, *Journal of Engineering Physics and Thermodynamics*, 64 (1993), 5, pp. 598-603
- [5] Diaz, S. H., *et al.*, Modeling of Thermal Response of Porcine Cartilage to Laser Irradiation, *IEEE J. of Selected Topics in Quantum Electronics*, 7 (2001), 6, pp. 944-951
- [6] Mcquiston, F. C., Parker, J. D., Spitler, J. D., Heating, Ventilating, and Air Conditioning, John Wiley and Sons Inc. 5th ed., New York, USA, 2000
- [7] Lewis, R. W., Morgan, K., Thomas, H. R., Seetharamu, K. N., The Finite Element Method in Heat Transfer Analysis, John Wiley and Sons Ltd., Chichester, UK, 1996
- [8] Jiang, S. C., Zhang, X. X., Effect of Dynamics Change of Tissue Properties during Laser-Induced Interstitial Thermotherapy, *Laser in Medical Science*, 19 (2005), 4, pp. 197-202
- [9] Zho, J. W., Herwig, H., Bio-Heat Analysis for Thermal Ablation of Biological Tissue During CW CO₂ Laser Irradiation, *Proceedings*, 13th International Heat Transfer Conference, Sydney, Australia, 2006, vol. 13, pp. BHT3